MedCrave
Step into the World of Research
Material Science & Engineering International Journal

Research Article
Open Access
CrossMark

The Effect of accelerator types on the phosphate Zn-%12Ni electrodeposite coating

Abstract

The aim of this study is to investigate the effect of nitrate and nitrite on the weight, morphology and electrochemical properties of phosphate Zn-%12Ni electrodeposited coatings. In order to investigate the phase structure and surface morphology of samples, X-ray diffraction and scanning electron microscopy were employed. Also, to measure the corrosion resistance behavior of the coats, Potentiostat/Galvanostat test was used. The results showed that nitrite accelerator reduces coating weight and surface porosity simultaneously obtaining by phosphating solution. Furthermore, coatings being obtained by the nitrite accelerator had a higher corrosion resistance than that of the nitrate accelerator.

Keywords: phosphate coating, nitrate, nitrite, porosity, electrodeposite coating

Volume 2 Issue 6 - 2018

Hafez Alizadeh,[1] Amir Hanaei,[2] Behzad Heidarshenas,[3] Armita Shahbazkhan,[4] Naghi Parvini Ahmadi,[1] Amirhossein Pakseresht[5]

[1]Department of Materials Engineering, Sahand University of Technology, Iran
[2]University of Tehran, Iran
[3]Nanjing University of Aeronautics and Astronautics, China
[4]Department of Materials Science and Engineering, Sharif University of Technology, Iran
[5]Department of Ceramics, Materials and Energy Research Center, Iran

Correspondence: Amirhossein Pakseresht, Center of Ceramic Coatings, Department of Ceramics, Materials and Energy Research Center, Karaj, Iran, Email amirh_pak@yahoo.com

Received: October 27, 2018 | **Published:** December 27, 2018

Introduction

As the matter of steel corrosion protection, Zinc electrodeposits have been vastly engaged.[1] These days, the corrosion resistance of conventional Zn coatings is not sufficient because the permanent industry requires (especially automotive and heavy duty applications like in hydraulic actuators) to reduce coating thickness and to increase the corrosion resistance of which at the same time. Therefore, extensive attempts have recently been made to develop highly corrosion resistant coatings on the steels and as a result, the conventional Zn coatings are being replaced by Zn alloys.[2–7] Zinc-nickel, zinc-iron, and zinc-cobalt are the most widely utilized alloys for coating, even though zinc-manganese, appeared to have an excellent corrosion resistance, is not commercially available.[8] It has been stated in several studies that corrosion resistance of electrodeposited Zn–Ni alloy coatings within a certain composition range (9–15 wt.%) can be significantly higher (5 to 6 times) than that of pure zinc.[8–21] The useful lifetime of Zn and Zn alloy electrodeposits can be further increased by the formation of a passive film on their surfaces which can even be applicable in high frequency microwave structures.[22–29] Chromate and phosphate films are common additional surface treatments used for various applications in different industrial fields.[26,30–39] An excellent anticorrosive behavior of chromate films is well known; however, the toxicity of Cr (VI) compounds restricts the application of this technology.[40] Phosphating is one of the most applicable processes carried out as a final surface treatment, although other methods like carburizing, nitriding and electrospary have been used.[30,41,43] Phosphate coatings, because of their low cost, high phosphating rate, very high corrosion resistance, high wear resistance, and good lubricant and cohesion properties, have attracted important role in automotive industry.[44] Short phosphating time is relatively an advantage for its application in industry. However, without any accelerator in the bath, the phosphating process would terminate in about 40 min. Therefore, such accelerators like nitride, nitrate, and chlorate should be added to zinc phosphate bath for accelerating and modifying the coating formation.[44–49] In the acidic bath, nitrate and nitrite react with hydrogen ions. The nitrate reduction is:[45]

$$NO_3^- + 2H^+ + 2e^- \rightarrow NO_2^- + H_2O \quad (1)$$

Nitrate in the bath and that produced by reaction (1) also has a reduction reaction like below:

$$NO_2^- + 2H^+ + 2e^- \rightarrow N_2 + O_2 + H_2O \quad (2)$$

On the ground that these two reactions consume H^+ rapidly, the local pH increase at the metal-solution interface can increase and facilitate the precipitation of insoluble phosphate,[45] quickly. In the present study, two phosphate baths were used for investigation of zinc nitrate and nitrite accelerator effects on the morphology and electrochemical properties of phosphate coatings.

Experimental

For phosphate coating, cylindrical steel samples with 10mm diameter and 10mm thickness were used. The compositions of the samples are listed in Table 1. For surface preparation, the samples were ground with sandpaper No 240-1000 first and then mechanical preparation was done to achieve uniform and suitable surface. In order to remove pollutions, oil, and corrosion products, degreasing by 60g/l NaOH at 60-70°C temperature for 20 minutes, and acid cleaning in 30% HCl solution for 1 minute at ambient temperature were carried out. Finally, to form the Zn-12Ni coating on samples, a bath with chemical composition and working condition as shown in Table 2 was used. In this research, two phosphate baths were used. Components and the operating conditions of phosphate baths are shown in Table 3. In general, phosphate coatings are porous; however, these porosities can be reduced by Chromic acid or its salts as a final treatment. Hence, an aqueous solution with 0.015% chromic acid was used. After phosphating, samples were immerged in the mentioned solution for 15 seconds at room temperature. Figure 1 shows schematic of phosphating process steps. For phase structure study, X-ray diffraction

(XRD) was performed with D8 advance diffractometer (Brokers) using Cu radiation (Cuk_{α}=1.54°A). The step-scan mode was 2–theta from 10° to 60° with a step size of 0.033°. The surface morphology of samples was investigated with CAMSCAN2300 Scanning electron microscopy (SEM). Coating weight as a main factor in determining the phosphate coating quality was measured for bath parameters and operating conditions standardization. The weight of the phosphate coating was determined by weighing the phosphated samples before and after stripping in 25g/l chromic acid solution for 2 minutes at 50°C temperature. The coating weight was calculated by applying the following equation:[45]

$$\text{Coating Weight}\left(\frac{g}{m^2}\right)=\frac{w_2-w_1}{\text{Coated Area}\left(cm^2\right)}\times 1000 \quad (3)$$

Table 1 Chemical composition of the steels used for phosphate coatings

Elements	Fe	C	P	S	N
%wt.	base	≥0.17	0.04	0.04	0.009

Table 2 Components and the operating conditions of the bath for Zn-12%Ni coating

Solution	Components (g/l)				Temperature (°C)	Time (min)	Current density (A/dm²)
Zn-12%Ni	$NiCl_2$	ZnO	NH_4Cl	$Na_4P_2O_7$	20	8	15
	5.59	14.35	160.47	133.82			

Table 3 Chemical composition and operating conditions of the phosphating baths

	ZnO(g/l)	H_3PO_4(cc/L)	HNO_3(cc/L)	$NaNO_3$(g/l)	$NaNO_2$(g/l)
Solution 1	10	17	6	1	-
Solution 2	11	18	7	-	1
pH			2.1-2.4		
Temperature (oC)			50±5		
Time (min)			10		

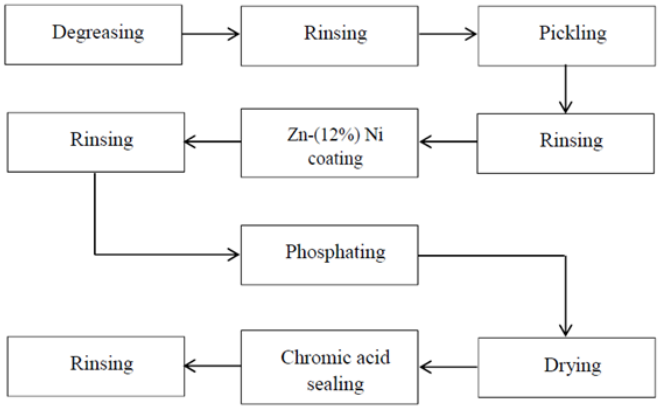

Figure 1 Flow chart depicting the operating sequence involved in phosphating process.

In which w_1, w_2 are sample weights after phosphating and stripping in chromic acid, respectively. The corrosion behavior of phosphate coatings was investigated in a 3.5% NaCl solution at 25°C. In this regard, a standard three electrode system with a Pt counter electrode, a saturated KCL reference electrode and a sample with the area of 0.785 cm^2 as working electrode were used. Samples were introduced into the cell system and allowed to reach open-circuit potential equilibrium (OCP) before electrochemical polarization measurements which took 1800s. Electrochemical polarization measurements were performed under potentiodynamic conditions; BEHPAJOOH BHP2063+ potentiostat/galvanostat with a potential scan rate of 0.001 V s^{-1}. After reaching OCP, Samples were polarized between ±300 mV around OCP. The corrosion current densities (i_{corr}) were determined by using the following equation:

$$i_{Corrosion}=\frac{b_a\times b_c}{2.3\times R_p\left(b_a+b_c\right)} \quad (4)$$

In which i_{corr} is the corrosion current density (A/cm^2), b_a and b_c are the anodic and cathodic Tafel slope (V/dcad), respectively, and R_p is the polarization resistance (Ω). As the corrosion reactions initiate at the coating-substrate interface, the reduction of phosphate films with reduced porosity is appreciated. Determination of porosity is an important task in controlling the quality of phosphate films. This parameter could be estimated by applying electrochemical measurements and by determining oxidation and reduction rates on the sample surface. By considering the phosphate coatings electrochemically inert at low anodic over potentials, the porosity of coatings was calculated by using the following equation.[33]

$$F(\%)=\left(\frac{R_{p,m}}{R_p}\right)10^{-\left|\Delta E_{corr.}\right|/b_a}\times 100 \quad (5)$$

Where F is the phosphate coating porosity (%), $R_{p.m}$ is the polarization resistance of the bare Zn–Ni (Ω), R_p is the polarization resistance of the phosphate Zn–Ni electrodeposits (Ω), ΔE_{corr} is the difference in E_{corr} of Zn–Ni electrode with and without phosphate layers (V), and b_a is the anodic Tafel slope of the bare Zn–Ni electrodeposits (V/dcad).

Result and discussion

Composition and surface morphology

X-ray diffraction patterns of the phosphated samples obtained by two phosphating solutions are shown in Figure 2. According to

these patterns, phosphate coating contains hopeite ($Zn_3(PO_4)_2.4H_2O$) and substrate (Ni_5Zn_{21}). Hopeite structure has a high adherence and corrosion resistance on the surface. SEM images of both phosphate coatings and Zn-Ni substrate without phosphate are shown in Figure 3. It can be observed that after phosphate coating, flower structure is formed on the surface. Hopeite structure looks like flowers[50,51] and also XRD results are in agreement with SEM results, meaning this phase is hopeite. By comparing both phosphate coatings, It can be perceived that phosphate coating resulted by the second solution had finer grains than that of the first one which is attributed to the presence of nitrite in the second solution. Nitrite leads to an increase in the reaction and the nucleation rate and eventually, causes a decrease in grain size of zinc phosphate. As the grain size decreases, flower structure with fine grains is formed (reactions 1 and 2). In principle, the structure of inorganic phosphate coatings depends on their weight. Normally, light-weight phosphate coatings (0.2–1.4 $g.m^{-2}$) have an amorphous structure, while middle-weight (1.4–7.5 $g.m^{-2}$) as well as a heavy-weight (7.5–30 $g.m^{-2}$) phosphate film demonstrate a crystalline structure[52].

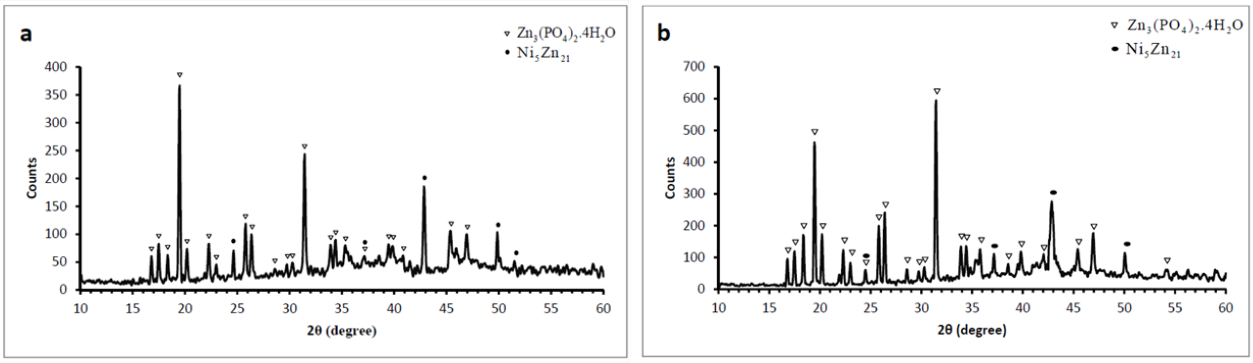

Figure 2 XRD patterns of the phosphate films on the Zn–Ni (12%) alloy surface. Coating produced by A) first solution B) second solution.

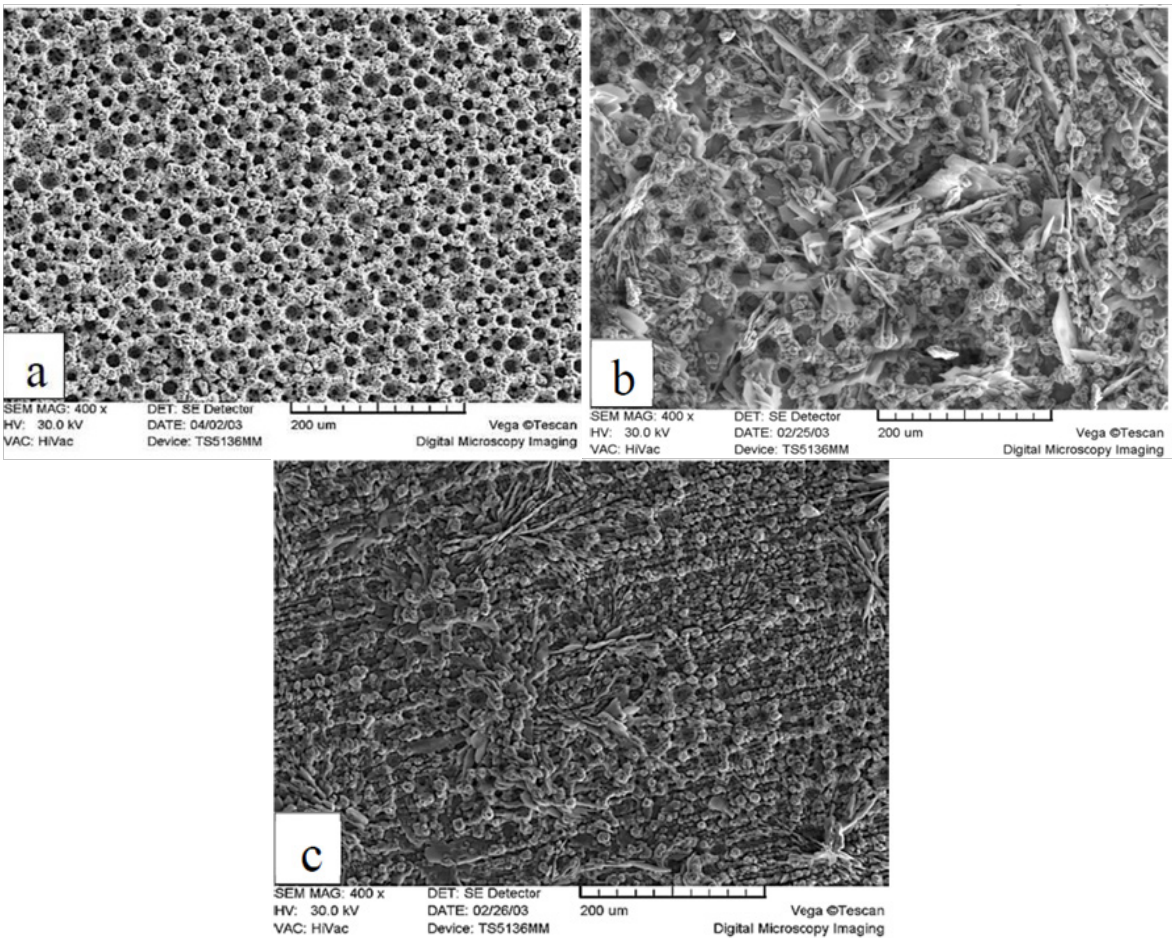

Figure 3 Scanning electron micrograph of Zn-Ni substrate A) without phosphate, B) with phosphate coating produced by first solution, and C) with phosphate coating produced by second solution.

Citation: Alizadeh H, Hanaei A, Heidarshenas B, et al. The Effect of accelerator types on the phosphate Zn-%12Ni electrodeposite coating. *Material Sci & Eng.* 2018;2(6):224–229. DOI: 10.15406/mseij.2018.02.00062

Coating weight

At 50°C and 10 minutes of immersion, coating weights of 7.095 and 11.086 g/m^2 were obtained for the second and first phosphate solution, respectively. Also as shown in XRD results, phosphate coatings produced by both solutions have a crystalline structure. It was proved from the values of weights that phosphate coating produced by the second solution has a lower weight than that obtained from the first solution. This weight difference is due to nitrite presence in the second phosphate solution. Nitrite increases the rate of phosphate reaction and decreases the amount of coating on the surface. By increasing the reaction rate, relatively uniform coating is formed on the surface. When the surface is covered by the coating, increase in the weight is not significant which is one of the conversion coating characteristics. In the acidic bath, nitrate in the first phosphate solution is reduced firstly, and then reduced nitrite from nitrate reduction reacts with hydrogen. In contrast, in the second phosphate solution nitride is present in the solution and this increases the reaction rate (Equations 1 and 2).

Corrosion behavior in a 3.5% NaCl solution

The corrosion behavior of Zn–Ni electrodeposits with/without phosphate coatings was evaluated by open-circuit (corrosion) potential (E_{corr}) monitoring and polarization measurements, carried out in a 3.5% NaCl solution. The values of i_{corr} and R_p were determined from polarization measurements. The obtained curves are presented in Figure 4 and the results are listed in Table 4. It can be seen from this data that the corrosion current density of Zn-Ni samples without phosphate coating is 2.551µcm^{-2}. The ratio of corrosion resistance with phosphate coating to that without phosphate coating is 9.48 and 10.85 for the first and second solutions, respectively. Phosphate coating decreases the corrosion current density (i_{corr}) and increases corrosion resistance in both solutions. The presence of hopeite structure on the surface as a suitable structure in phosphate coating causes an increase in the corrosion resistance of the coating. Also, it is noticed that the amount of i_{corr} for phosphate coating produced by the second solution is lower than the first solution, and therefore, its corrosion resistance increases. Also, it is seen that i_{corr} for phosphate coating produced by the second solution is lower than the first one, and eventually, the corrosion resistance of this coating is higher (Table.4). This behavior of the phosphate coating produced by the second solution can be explained by the fine grain structure of the coating. Surface of coating have a uniform and fine grain structure in the presence of nitrite. Likewise, surface porosity decreases, and hence, the contact between corrosive material and substrate was prevented, resulting in an increase in corrosion resistance.

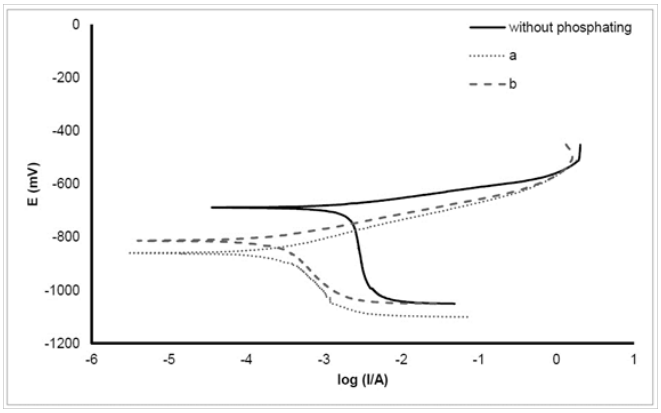

Figure 4 Potentiodynamic polarization curves of the phosphated and non-phosphated Zn–Ni alloy electrodes in a 3.5% NaCl solution at 25±2°C. Potential scan rate is 0.001 V s^{-1}.

Table 4 The electrochemical parameters (corrosion current i_{corr}, polarization resistance R_p, the difference of E_{corr} between Zn–Ni electrode with and without phosphate layers ΔE_{corr}, anodic and Cathodic Tafel slope b_a, b_c) of phosphate Zn–Ni alloy electrodes, measured in a 3.5% NaCl solution.

Phosphate coating type	icorr (µA/cm^2)	Rp (kΩ).cm^2	(-) Ecorr (mV)	ba(mV/dcad)	(-)bc (mV/dcad)	ΔEcorr(mV)
Without	2.551	8.676	688	53.09	1237	-
1	0.269	89.309	859	67.7	300.7	171
2	0.2351	87.678	812	56.03	308.5	124

Coating porosity

After immersion in solutions at 50°C for 10 minutes, the porosity was %0.000519 and 0.0116 for the second and first solutions, respectively, which are lower than %1, showing the excellent quality of produced coats. The obtained values for the phosphate coating porosities are in the good agreement with the results of corrosion behavior of phosphate Zn–Ni alloy in 3.5% NaCl solution (Table 4). The obtained data indicate that the protective abilities of phosphate coatings on Zn–Ni electrodeposits in 3.5% NaCl solution depend mainly on their porosities. In general, it can be concluded that the lower porosity on the surface, the lower corrosion rate and the higher corrosion resistance of the substrate would be. Porosity in the coating obtained by the second solution is lower than that of the first solution which has to do with the presence of nitrite. Nitrite causes an increase in the phosphate reactions and insoluble phosphate production rates on the surface, resulting in a decrease in surface porosity.

Conclusion

The effects of nitrite and nitrate accelerators on the properties of phosphate Zn-%12Ni electrodeposited coatings were investigated. Hopeite $Zn_3(PO_4)_2.4H_2O$ was the dominant structure in the phosphate coatings produced by both solutions. The type of accelerator had no effect on the obtained structure. Nitrite accelerator increases the formation rate of insoluble phosphate in comparison with nitrate, resulting in a low weight coating from nitrate solution. Compared to the coating produced by nitrate solution, the corrosion resistance of the coating obtained by nitrite solution is higher, notwithstanding lower weight value of the coating obtained by nitrite solution. Due to its low porosity value, the corrosion resistance of the coating obtained by nitrite solution is high. The protective properties of the phosphate coatings are related principally to their porosities. The low value of porosity is beneficial for the corrosion resistance enhancement since a phosphate layer acts as a physical barrier against corrosive agents.

Acknowledgments

None.

Conflicts of interest

Author declares that there is no conflicts of interest.

Citation: Alizadeh H, Hanaei A, Heidarshenas B, et al. The Effect of accelerator types on the phosphate Zn-%12Ni electrodeposite coating. *Material Sci & Eng.* 2018;2(6):224–229. DOI: 10.15406/mseij.2018.02.00062

References

1. Ashiru O, Shirokoff J. Electrodeposition and characterization of tin-zinc alloy coatings. *Applied surface science*. 1996;103(2):159–169.
2. Karimi M, Solati N, Ghasemi A, et al. Carbon nanotubes part II: a remarkable carrier for drug and gene delivery. *Expert opinion on drug delivery*. 2015;12(7):1089–1105.
3. Alizadeh H, Hanaei A, Pakseresht A, et al. Effect of Ca2+ additives on morphology, composition and corrosion resistant of Zn–12% Ni phosphate coating. *Journal of Materials Research and Technology*. 2016;5(4):327–332.
4. Baniasadi F, Bahmannezhad B, Nikpoor N, et al. Thermal stability investigation of expanded martensite. *Surface and Coatings Technology*. 2016;300:87–94.
5. Sharifi S, Rezaei SM, Tivay A, et al. Multi-class fault detection in electro-hydraulic servo systems using support vector machines. Paper presented at: Robotics and Mechatronics (ICROM), 2016 4th International Conference. 2016.
6. Sharifi S, Tivay A, Rezaei SM, et al. Leakage fault detection in Electro-Hydraulic Servo Systems using a nonlinear representation learning approach. *ISA Transactions*. 2018;73:154–164.
7. Pirbazari PM, Kisomi BF. Co/TiO_2 nanoparticles: preparation, characterization and its application for photocatalytic degradation of methylene blue. *Desalin, Water Treat*. 2017;63:283–292.
8. Wilcox G, Gabe D. Electrodeposited zinc alloy coatings. *Corrosion Science*. 1993;35(5):1251–1258.
9. Gavrila M, Millet J, Mazille H, et al. Corrosion behaviour of zinc–nickel coatings, electrodeposited on steel. *Surface and coatings technology*. 2000;123(2):164–172.
10. Ramanauskas R. Structural factor in Zn alloy electrodeposit corrosion. *Applied surface science*. 1999;153(1):53–64.
11. Ramanauskas R, Juškėnas R, Kaliničenko A, et al. Microstructure and corrosion resistance of electrodeposited zinc alloy coatings. *Journal of Solid State Electrochemistry*. 2004;8(6):416–421.
12. Fedrizzi L, Fratesi R, Lunazzi G, et al. Field and laboratory corrosion tests on zinc-nickel alloy coatings. *Surface and Coatings Technology*. 1992;53(2):171–176.
13. Kautek W, Sahre M, Paatsch W. Transition metal effects in the corrosion protection of electroplated zinc alloy coatings. *Electrochimica acta*. 1994;39(8):1151–1157.
14. Bajat J, Maksimović M, Mišković-Stanković V, et al. Electrodeposition and characterization of Zn–Ni alloys as sublayers for epoxy coating deposition. *Journal of applied electrochemistry*. 2001;31(3):355–361.
15. Malekzad H, Mirshekari H, Sahandi Zangabad P, et al. Plant protein-based hydrophobic fine and ultrafine carrier particles in drug delivery systems. *Critical Reviews in Biotechnology*. 2017:1–21.
16. Yarahmadi M, Goudarzi HM, Shafii M. Experimental investigation into laminar forced convective heat transfer of ferrofluids under constant and oscillating magnetic field with different magnetic field arrangements and oscillation modes. *Experimental Thermal and Fluid Science*. 2015;68:601–611.
17. Mozaffari S. Rheology of Bitumen at the Onset of Asphaltene Aggregation and its Effects on the Stability of Water-in-Oil Emulsion. University of Alberta; 2015.
18. Najdahmadi A, Zarei-Hanzaki A, Farghadani E. Mechanical properties enhancement in Ti–29Nb–13Ta–4.6 Zr alloy via heat treatment with no detrimental effect on its biocompatibility. *Materials & Design*. 2014;54:786–791.
19. Ebrahimian Pirbazari A, Fakhari Kisom B, Ghamangiz Khararoodi M. Anionic surfactant-modified rice straw for removal of methylene blue from aqueous solution. *Desalination and Water Treatment*. 2016;57(39):18202–18216.
20. Nazari A, Farhad S. Heat generation in lithium-ion batteries with different nominal capacities and chemistries. *Applied Thermal Engineering*. 2017;125:1501–1517.
21. Nazari A, Esmaeeli R, Hashemi SR, et al. The effect of temperature on lithium-ion battery energy efficiency with graphite/$LiFePO_4$ electrodes at different nominal capacities. ASME 2018 Power Conference collocated with the ASME 2018 12th International Conference on Energy Sustainability and the ASME 2018 Nuclear Forum 2018. 2018.
22. Pech-Canul M, Ramanauskas R, Maldonado L. An electrochemical investigation of passive layers formed on electrodeposited Zn and Zn-alloy coatings in alkaline solutions. *Electrochimica acta*. 1997;42(2):255–260.
23. Oghbaei M, Baniasadi F, Asgari S. Lithium iron silicate sol–gel synthesis and electrochemical investigation. *Journal of Alloys and Compounds*. 2016;672:93–97.
24. Goudarzi HM, Yarahmadi M, Shafii MB. Design and construction of a two-phase fluid piston engine based on the structure of fluidyne. *Energy*. 2017;127:660–670.
25. Hokmabad BV, Sadri B, Faraji S, et al. Experimental investigation of electrospraying of water and KCl aqueous solutions in dielectric media.
26. Mirab F, Eslamian M, Bagheri R. Fabrication and characterization of a starch-based nanocomposite scaffold with highly porous and gradient structure for bone tissue engineering. *Biomedical Physics & Engineering Express*. 2018;4(5):055021.
27. Nazari A. Heat Generation in Lithium-ion Batteries. University of Akron; 2016.
28. Loghmannia P, Kamyab M, Nikkhah MR, et al Analysis and design of a low sidelobe level and wide-band aperture coupled microstrip antenna array using FDTD. Electrical Engineering (ICEE), 2013 21st Iranian Conference on 2013. 2013.
29. Nikkhah MR, Loghmannia P, Rashed-Mohassel J, et al. Theory of ESPAR design with their implementation in large arrays. *IEEE Transactions on Antennas and Propagation*. 2014;62(6):3359–3364.
30. Sinha P, Feser R. Phosphate coating on steel surfaces by an electrochemical method. *Surface and Coatings Technology*. 2002;161(2):158–168.
31. Townsend H, Hart R. Composition of Chromate Passivation Films on Aluminum□Zinc Alloy□Coated Sheet Steel. *Journal of The Electrochemical Society*. 1984;131(6):1345–1348.
32. Rebeyrat S, Grosseau-Poussard J, Silvain JF, et al. Phosphating of bulk α-iron and its oxidation resistance at 400°C. *Applied surface science*. 2002;199(1):11–21.
33. Girčienė O, Gudavičiūtė L, Juškėnas R, Ramanauskas R. Corrosion resistance of phosphated Zn–Ni alloy electrodeposits. *Surface and Coatings Technology*. 2009;203(20):3072–3077.
34. Long Z, Zhou Y, Xiao L. Characterization of black chromate conversion coating on the electrodeposited zinc–iron alloy. *Applied Surface Science*. 2003;218(1):124–137.
35. Flis J, Mańkowski J, Zakroczymski T, Bell T. The formation of phosphate coatings on nitrided stainless steel. *Corrosion science*. 2001;43(9):1711–1725.

Citation: Alizadeh H, Hanaei A, Heidarshenas B, et al. The Effect of accelerator types on the phosphate Zn-%12Ni electrodeposite coating. *Material Sci & Eng.* 2018;2(6):224–229. DOI: 10.15406/mseij.2018.02.00062

36. Mozaffari S, Tchoukov P, Atias J, et al. Effect of asphaltene aggregation on rheological properties of diluted athabasca bitumen. *Energy & Fuels*. 2015;29(9):5595–5599.

37. Mozaffari S, Tchoukov P, Mozaffari A, et al. Capillary driven flow in nanochannels–Application to heavy oil rheology studies. *Colloids and Surfaces A: Physicochemical and Engineering Aspects*. 2017;513:178–187.

38. Najdahmadi A, Lakey JR, Botvinick E. Diffusion coefficient of alginate microcapsules used in pancreatic islet transplantation, a method to cure type 1 diabetes. Nanoscale Imaging, Sensing, and Actuation for Biomedical Applications XV2018.

39. Najdahmadi A, Lakey JR, Botvinick E. Structural Characteristics and Diffusion Coefficient of Alginate Hydrogels Used for Cell Based Drug Delivery. *MRS Advances*. 2018:1–10.

40. Svensson JE, Johansson LG. A laboratory study of the effect of ozone, nitrogen dioxide, and sulfur dioxide on the atmospheric corrosion of zinc. *Journal of The Electrochemical Society*. 1993;140(8):2210–2216.

41. Faraji S, Sadri B, Hokmabad BV, et al. Experimental study on the role of electrical conductivity in pulsating modes of electrospraying. *Experimental Thermal and Fluid Science*. 2017;81:327–335.

42. Faraji S, Sadri B, Hokmabad BV, et al. Electrospray characteristics of aqueous KCl solutions with various electrical conductivities.

43. Hashemi SR, Nazari A, Esmaeeli R, et al. Fast fault diagnosis of a lithium-ion battery for hybrid electric aircraft. Proceedings of the ASME 2018 Power and Energy Conference 2018. 2018.

44. Biestek T, Weber J. Electrolytic and chemical conversion coatings: a concise survey of their production, properties and testing: Portcullis Press Limited; 1976.

45. Niu L, Jiang Z, Li G, et al. A study and application of zinc phosphate coating on AZ91D magnesium alloy. *Surface and Coatings Technology*. 2006;200(9):3021–3026.

46. Banczek E, Rodrigues P, Costa I. The effects of niobium and nickel on the corrosion resistance of the zinc phosphate layers. *Surface and Coatings Technology*. 2008;202(10).

47. Zimmermann D, Munoz A, Schultze J. Microscopic local elements in the phosphating process. *Electrochimica acta*. 2003;48(20):3267–3277.

48. Woods KJ. Accelerator for phosphating solutions: Google Patents; 1978.

49. Keshmiri K, Mozaffari S, Tchoukov P, et al. Using Microfluidic Device to Study Rheological Properties of Heavy Oil. arXiv preprint. 2016.

50. Arnaud Y, Sahakian E, Romand M, et al. Study of hopeite coatings: I. Pure hopeite thermal dehydration: dihydrate, Zn3 (PO4) 2• $2H_2O$, structure conformation. *Applied surface science*. 1988;32(3):281–295.

51. Arnaud Y, Sahakian E, Lenoir J, et al. Study of hopeite coatings: II. Study of polycationic hopeites: structure and dehydration process. *Applied surface science*. 1988;32(3):296–308.

52. Weng D, Jokiel P, Uebleis A,et al. Corrosion and protection characteristics of zinc and manganese phosphate coatings. *Surface and Coatings Technology*. 1997;88(1):147–156

Citation: Alizadeh H, Hanaei A, Heidarshenas B, et al. The Effect of accelerator types on the phosphate Zn-%12Ni electrodeposite coating. *Material Sci & Eng.* 2018;2(6):224–229. DOI: 10.15406/mseij.2018.02.00062